Applied Catalysis B: Environmental 138–139 (2013) 95–103

Contents lists available at SciVerse ScienceDirect

Applied Catalysis B: Environmental

journal homepage: www.elsevier.com/locate/apcatb

Synthesis, characterization and photocatalytic activity of visible-light plasmonic photocatalyst AgBr-$SmVO_4$

Tingting Li[b], Yiming He[a,*], Hongjun Lin[c], Jun Cai[a], Lvzhuo Dong[b], Xiaoxing Wang[a], Mengfei Luo[b], Leihong Zhao[b,*], Xiaodong Yi[d], Weizheng Weng[d]

[a] Department of Materials Physics, Zhejiang Normal University, Jinhua 321004, China
[b] Institute of Physical Chemistry, Zhejiang Key Laboratory for Reactive Chemistry on Solid Surfaces, Zhejiang Normal University, Jinhua 321004, China
[c] College of Geography and Environmental Sciences, Zhejiang Normal University, Jinhua 321004, China
[d] State Key Laboratory Physical Chemistry of Solid Surfaces, Xiamen University, Xiamen 361005, China

ARTICLE INFO

Article history:
Received 18 November 2012
Received in revised form 24 January 2013
Accepted 3 February 2013
Available online 26 February 2013

Keywords:
$AgBr/SmVO_4$
Visible light irradiation
Composite
Plasmon

ABSTRACT

A novel composite photocatalyst AgBr-$SmVO_4$ was synthesized by deposition method and characterized by X-ray diffraction (XRD), scanning electron microscopy (SEM), transmission electron microscopy (TEM), X-ray photoelectron spectroscopy (XPS), and UV–vis diffuse reflectance spectroscopy (DRS). The XRD, TEM, and XPS results indicated the prepared sample was actual a three-phase composite: $SmVO_4$, AgBr, and Ag during the photocatalytic reaction. Due to the plasmon effect of Ag nanoparticles, the composite exhibited excellent photoabsorption ability for visible light. The photoelectrochemical measurement verified that the suitable band potential of AgBr and $SmVO_4$ and the existence of metal Ag resulted in the high efficiency in charge separation of the composite. Photocatalytic degradation of rhodamine B (RhB) was carried out to evaluate the photocatalytic activity of $AgBr/SmVO_4$ under visible-light irradiation. The composite presented excellent photocatalytic activity due to the synergetic effect of $SmVO_4$, AgBr, and Ag nanoparticles. The photocatalytic activities of AgBr-$SmVO_4$ were differently affected by the AgBr content in the catalyst, AgBr-$SmVO_4$ amount, initial RhB concentration, and light sources. The highest degradation rate of 0.150 min^{-1} was obtained on the 50 wt% AgBr-$SmVO_4$ sample, which was respectively 3.8 times and 25 times higher than that of AgBr and $SmVO_4$ photocatalyst. It was found that $^{\bullet}O_2^-$ and Br^0 acted as the main reactive species for the degradation of RhB under visible-light irradiation.

1. Introduction

The problem of environmental pollution caused by organic and toxic wastes have drawn more and more attention during the past several decades. Many conventional methods such as catalytic combustion, reverse osmosis, and activated carbon adsorption have been used to deal with these pollutants in air or water surroundings. However, many drawbacks still existed in these methods because of their expensiveness and the increasing number of refractory pollutants. Recent researches showed that heterogeneous photocatalytic oxidation technologies were the promising methods [1,2]. Among all the photocatalytic materials previously reported, TiO_2 semiconductor has been attached significantly scientific interest because of its unique characteristics in chemical stability and high activity [3,4]. However, TiO_2 can only absorb the ultraviolet light (4% of the solar light spectrum) due to its large band gap, which greatly limits its practical application in a large scale. Therefore, designing a novel photocatalyst that could highly utilize the solar energy has become an imperative topic in the current photocatalysis field.

Recently, Ag/AgX (X = Cl, Br, I) plasmonic photocatalysts have inspired many researchers' interest due to their high photocatalytic activity [5–9]. Silver halides are photosensitive materials extensively used as source materials in photographic films. Under light irradiation, they are instable because the photogenerated electrons can reduce the interstitial Ag^+ to Ag^0 cluster. Therefore, silver halides are seldom used as photocatalysts. However, Kakuta et al. reported a stable photocatalyst $AgBr/SiO_2$ which could be used for H_2 generation in CH_3OH/H_2O solution [10]. Although Ag^0 was detected by X-ray diffraction analysis after the reaction, H_2 generation was observed and hydrogen was continuously evolved for 200 h without destruction of AgBr. It can be attributed to that the formed Ag nanoparticles on the surface of AgBr act as efficient electron traps and subsequently suppress the decomposition of AgBr. Moreover, the formed Ag nanoparticles present strong UV–vis absorption due to the surface plasmonic resonance (SPR) effect [11,12]. Hence, Ag/AgX can be expected to be a stable photocatalyst with high photoabsorption performance. This hypothesis has been

* Corresponding authors. Tel.: +86 0579 83792294; fax: +86 0579 83714946.
E-mail addresses: hym@zjnu.cn, he_yiming@163.com (Y. He), zhaoleihong@163.com (L. Zhao).

0926-3373/$ – see front matter © 2013 Elsevier B.V. All rights reserved.
http://dx.doi.org/10.1016/j.apcatb.2013.02.024

recently verified by the work of Wang et al. [5–9] who reported that both Ag@AgCl and Ag@AgBr are highly efficient and stable photocatalyst under visible light.

Since the destruction of AgX can be restrained by trapping the photogenerated electrons, it means that the coupling of AgX by a semiconductor with suitable band potential can promote the stability of AgX. In these composite systems, the conduction band (CB) bottom of coupled semiconductor lies below the CB bottom of AgX. The photoinduced electrons at the CB bottom of AgX can migrate to that of semiconductor due to the difference in band potential. The migration not only suppresses the reduction of Ag^+, but also prolongs the lifetime of charge carriers which is beneficial for the photocatalytic reaction. Of course, the partial decomposition of AgX is unavoidable since the combination of Ag^+ with electrons is faster than the process of charge transfer. Therefore, the AgX-semiconductor system is actual Ag-AgX-semiconductor photocatalyst. Due to the double charge transfer in the system, the composite photocatayst presents excellent photocatalytic activity both in dye degradation and CO_2 reduction [13–19]. For example, Wang et al. prepared $H_2WO_4{\cdot}H_2O$/Ag/AgCl composite nanoplates which exhibited a much higher photocatalytic activity than the one-component ($H_2WO_4{\cdot}H_2O$) or two-component (Ag/AgCl and $H_2WO_4{\cdot}H_2O$/Ag) photocatalysts in methyl orange (MO) degradation [13]. Asi et al. prepared Ag-AgBr-TiO_2 photocatalyst and tested its photocatalytic performance in CO_2 reduction [14]. The results showed that the composite had relatively high reduction yields under visible-light irradiation. Similar plasmonic catalysts, such as Ag-AgX (X = Br, Cl)-WO_3 [15,16], Ag-AgCl-$BiVO_4$ [17], Ag/AgCl/$W_{18}O_{49}$ [18], AgX (X = Br, Cl)/g-C_3N_4 [19], Ag-AgCl-BiOCl [20], AgI/ZnO [21], and Ag/AgCl/graphene [22], have been reported. However, the demand for the photocatalytic activities is still not satisfied. More efficient photocatalytic structures need to be developed.

Herein, a novel AgBr-$SmVO_4$ composite was constructed and synthesized by a facile precipitation method. $SmVO_4$ nanoparticles were chosen as the important component due to its suitable band potential and facile preparation [23]. The prepared samples showed high visible light photocatlaytic activity for the photocatalytic degradation of rhodamine B (RhB) aqueous solution. Furthermore, the roles of different reactive species were studied, and a charge transfer mechanism was also discussed.

2. Experimental

2.1. Preparation of catalysts

NH_4VO_3 (>99%), $Sm(NO_3)_3{\cdot}6H_2O$ (>99%), $AgNO_3$ (>99.8%), NaBr (>99%), NaOH (>96.0%), $Ti(OBu)_4$ (>98.5%), $CO(NH_2)_2$ (>99.0%), and P25 as reference were purchased commercially without further purification. Pure $SmVO_4$ and nitrogen doped TiO_2 (N-TiO_2) were prepared according to our previous study [23,24]. Pure AgBr was prepared as follows: solution of $AgNO_3$ and NaBr with an Ag to Br mole ratio of 1:1 were mixed to get a yellow deposit. After aged at room temperature for 2 h, the deposit was filtered, washed three times by water, and dried at 60 °C for 12 h.

AgBr-$SmVO_4$ composites were prepared by a deposition method. In a typical run, solutions of NH_4VO_3 and $Sm(NO_3)_3$ were first mixed to get a yellow deposit. The pH value of the solution was adjusted to 7 by a solution of NH_3. Then, different stoichiometric amounts of $AgNO_3$ and NaBr solution were added successively into the above suspension under constant stirring. After addition, the mixtures were vigorously stirring for 5 h. The theoretical weight percentages of AgBr/($SmVO_4$ + AgBr) were controlled to be 20 wt.%, 40 wt.%, 50 wt.%, 60 wt.%, and defined as AS-20, AS-40, AS-50, AS-60, respectively. Finally, the precipitates were successively collected, washed with deionized water for three times, dried at 60 °C for 24 h, and calcined at 500 °C for 2 h.

2.2. Characterizations

The XRD characterization of catalysts was carried out on Philips PW3040/60 using Cu Kα radiation (40 kV/40 mA). The Fourier transform infrared spectroscopy (FT-IR) spectra of the catalysts were recorded on Nicolet NEXUS670 with a resolution of 4 cm^{-1}. The specific surface areas were measured on Autosorb-1 (Quantachrome Instruments) by the Brunauer–Emmett–Teller (BET) method. The SEM pictures were taken on a field emission scanning electron microscope (Hitachi S-4800). The TEM images were collected with a JEOL 2100F transmission electron microscope at an accelerating voltage of 200 kV. The UV–vis diffuse reflectance spectra (DRS) of catalysts were recorded on a UV–vis spectrometer (Thermo Nicolet Evolution 500) equipped with an integrating sphere. The X-ray photoelectron spectroscopy (XPS) measurements were performed with a Quantum 2000 Scanning ESCA Microprobe instrument using Al Kα. The C 1s signal was set to a position of 284.6 eV.

2.3. Photoelectrochemical (PC) measurement

To investigate the transition of photogenerated electrons in AgBr-$SmVO_4$ composite, AgBr and AS-50 composite electrodes were prepared according to the previous study [25]. The photocurrents were measured with an electrochemical analyzer (CHI660B) in a standard three-electrode system under zero bias. The prepared sample, a Pt wire, and Ag/AgCl (saturated KCl) work as the working electrode, the counter electrode, and the reference electrode, respectively. A 500 W Xe arc lamp through a UV-cutoff filter ($\lambda > 420$ nm) served as a light source. Na_2SO_4 (0.5 mol/L) aqueous solution was used as the electrolyte.

2.4. Photocatalytic experiments

The photocatalytic activities of AgBr-$SmVO_4$ composites were tested by the degradation of RhB under visible light irradiation. A 350 W Xe lamp was used as the light source. Two optical filters were used to eliminate the UV light and infrared light (800 nm > λ > 420 nm). The power density of light at the position of reactor was about 7.4 mW/cm^2. Other filters ($\lambda > 460$ nm, $\lambda > 535$ nm, $\lambda > 560$ nm) were also used to cutoff the light with higher wavelength. In each experiment, 0.2 g catalyst powder was added in aqueous solution of RhB (100 mL, 20 mmol/L) in a vessel. Prior to irradiation, the suspensions were magnetically stirred in dark for 60 min. During the RhB photodecomposition, samples were withdrawn at regular intervals and centrifuged to separate solid particles for analysis. The concentration of aqueous RhB was determined by measuring its absorbance at the range of 400–700 nm. The RhB degradation was calculated by Lambert–Beer equation. Photoactivities for RhB in the dark in the presence of the photocatalyst and under visible-light irradiation in the absence of the photocatalyst were also evaluated. The photodegration of phenol and other dyes, methyl orange (MO), methylene blue (MB), and malachite green (MG), were also carried out by the similar procedure.

The examination experiment process of reactive species was similar to the photodegradation experiment. A quantity of scavengers was introduced into the RhB solution prior to addition of the catalyst. The concentration of scavengers was controlled to be 0.2 mol/L according to the previous studies [26,27].

Terephthalic acid photoluminescence probing technique (TA-PL) was used in the detection of •OH radicals [24,28]. In the detection experiment, a basic TA solution was added to the reactor instead of RhB and the concentration of TA was set at 5×10^{-3} mol/L

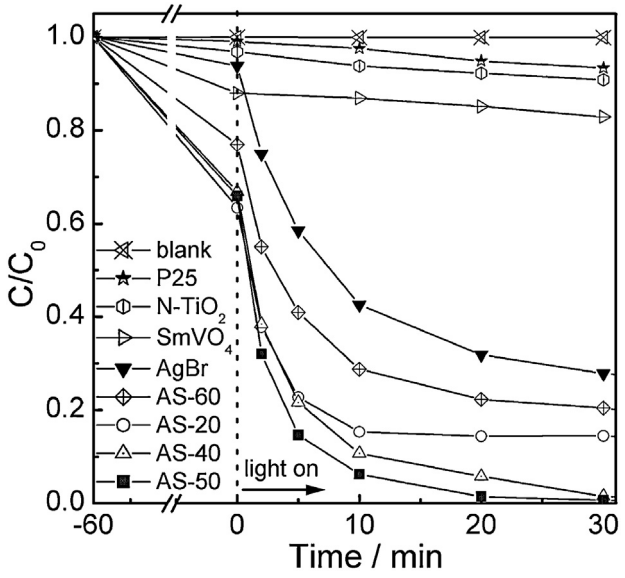

Fig. 1. Photocatalytic activities of AgBr-$SmVO_4$ composites on photodegradation of RhB under visible-light irradiation.

in 1×10^{-2} mol/L NaOH solution. The photoluminescence (PL) spectra were collected on FLS-920 spectrometer (Edinbergh Instrument), using a Xe lamp (excitation at 316 nm) as light source.

3. Results and discussion

3.1. Photocatalytic activity

The degradation of RhB under visible-light irradiation was used to evaluate the photoactivity of AgBr-$SmVO_4$ composite. For each run, before irradiation, the reaction solution was first magnetically stirred in dark for 60 min to achieve adsorption and/desorption equilibrium, which has been proven by the adsorption experiment (See Fig. S1). Fig. 1 shows the changes of the RhB concentration versus the reaction time over the AgBr-$SmVO_4$ catalysts. As shown in Fig. 1, the photolysis of RhB under visible light is negligible. P25 presents a poor photoactivity which could be attributed to the photosensitization effect of RhB since P25 could only absorb the UV light. Besides, it also indicated that the contribution of the dye photosensitization effect was very limited. The photoactivity of N-TiO_2 was slightly higher than that of P25. For $SmVO_4$, the concentration of RhB decreased to 23% of the initial value after 60 min of adsorption and 30 min of visible-light irradiation, which could be mainly attributed to its better adsorption for RhB compared with P25 and N-TiO_2. The RhB adsorption ability of AgBr was lower than that of $SmVO_4$, resulting in less than 9% of RhB adsorption after 60 min stirring. However, when the suspension was irradiated under visible light, the RhB concentration decreased quickly. Since AgBr would transform to Ag/AgBr system at the beginning of reaction, the high photoactivity could be mainly ascribed to the surface plasma effect of Ag nanoparticles [5–7]. The coupling of AgBr with $SmVO_4$ dramatically promoted both the dye adsorption and photocatalytic activity. The AS-20 sample had the highest adsorption ability (Fig. 1 and Fig. 1S), and the AS-50 composite displayed the highest photocatalytic activity. Under visible-light illumination for 30 min, the RhB concentration decreased to 0.006% of the initial concentration in the presence of AS-50 sample. Its degradation rate is 0.150 min^{-1}, which is 3.8 times higher than that of AgBr photocatalyst (See Fig. S2). FT-IR experiment of the used sample and chemical oxygen demand (COD) measurements of the RhB solution were performed to verify whether dye was completely degraded. No organics was

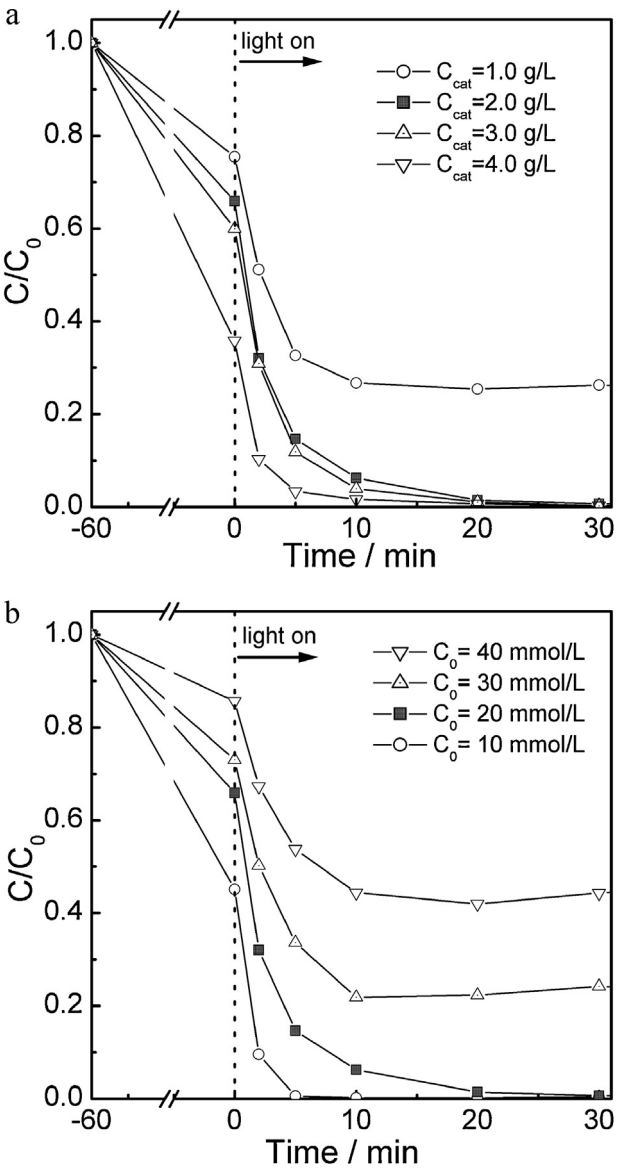

Fig. 2. Effect of catalyst content and initial dye concentration on the degradation of RhB.

observed on the FT-IR spectrum of the used AS-50 sample, indicating the adsorbed RhB was also degraded (See Fig. S3). The COD result further showed that 98.0% of RhB was completely degraded to carbonate, which is much larger than that of N-TiO_2 (See Fig. S4). It is clear that the synthesized AgBr/$SmVO_4$ composite possesses both excellent activity and high complete oxidation ability.

The AS-50 sample was then employed for the following investigations due to its high photoactivity. Photocatalyst amount is one of the critical parameters of the degradation efficiency of dyes. Fig. 2 shows the effect of AS-50 content on the degradation efficiency of RhB. It can be seen that the degradation efficiency of RhB enhanced first with the increase of catalyst amount, and then leveled off the highest value of 4.0 g/L. The increased degradation efficiency can be mainly attributed to the enhanced adsorption of RhB. Besides, higher AgBr-$SmVO_4$ content indicates more active sites that can absorb photons to generate much more active species, which also promote the degradation of RhB. However, the increase in catalyst content would not always be beneficial for the dye degradation due to the reduction in the penetration of light and light scattering by

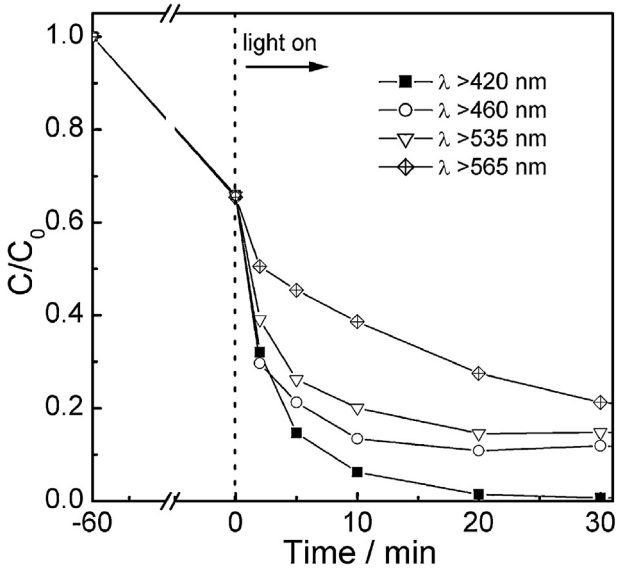

Fig. 3. Photocatalytic degradation of RhB under light with different wavelengths.

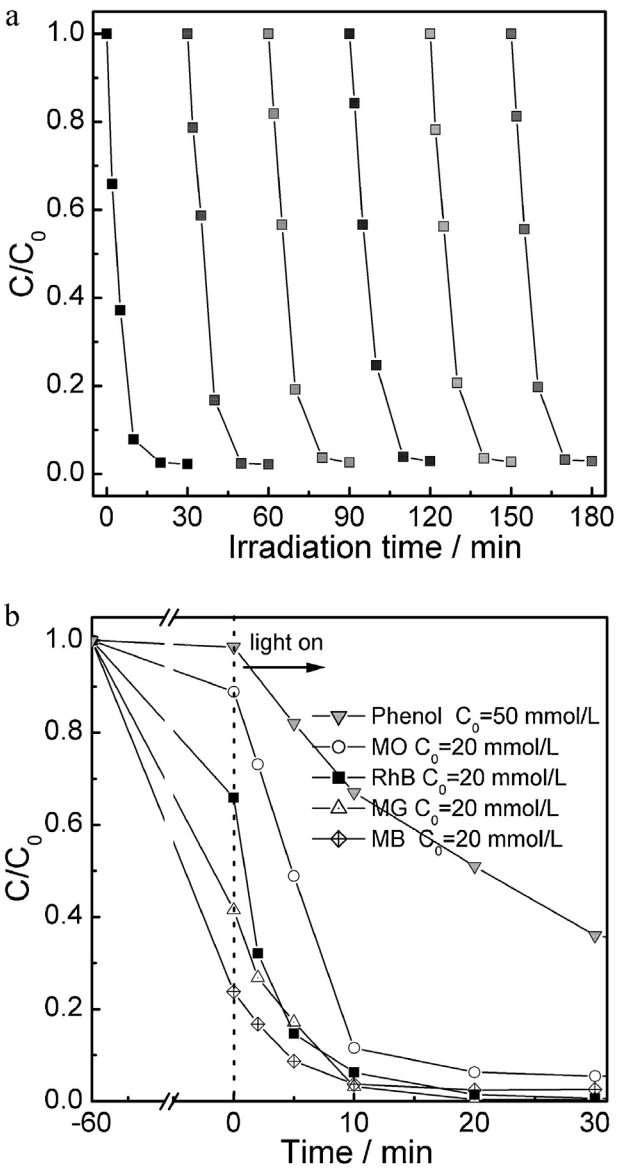

Fig. 4. Cycling runs for the photodegradation of RhB (a) and the photodegradation of different organics (b) in the presence of AS-50 sample under visible light irradiation.

catalyst [29]. Considering the cost of catalyst, 2.0 g/L is a suitable content for the AgBr-$SmVO_4$ photocatalyst.

Fig. 2b shows the effect of the initial concentration of RhB on the photocatalytic activity. The photodegradation rate decreased with the increase of initial dye concentration. The possible reason is the visible light screening effect of the dye. When the RhB concentration is high, a significant amount of visible light may be absorbed by the RhB molecules rather than by the AgBr-$SmVO_4$ catalyst and thus the efficiency of the catalytic reaction is reduced.

The influence of the light source on the photocatalytic rate was also investigated. Four optical filters with $\lambda > 420$ nm, $\lambda > 460$ nm, $\lambda > 535$ nm, and $\lambda > 565$ nm were used to cut off the unwanted light. The power density of the light at the position of catalysts was 7.4 mW/cm^2 ($\lambda > 420$ nm), 6.3 mW/cm^2 ($\lambda > 460$ nm), 5.8 mW/cm^2 ($\lambda > 535$ nm), and 5.1 mW/cm^2 ($\lambda > 560$ nm), respectively. The testing results are shown in Fig. 3. The photoactivity of AS-50 sample decreased with the increase of the cut-off wavelengths. One possible reason for such a result is the decreased visible-light intensity, which is unfavorable for the absorption of photons for catalyst and the formation of electron–hole pairs, and therefore decreases the degradation efficiency of RhB. Another possible reason is the limited optical property of catalyst. For example, $SmVO_4$ can only absorb the light with $\lambda < 543$ nm [24]. Under the illumination of light with $\lambda > 543$ nm, no photoactivity would be detected on $SmVO_4$. Anyway, although the decrease in photoactivity was observed, the AS-50 sample still displayed a high photoactivity under light with $\lambda > 565$ nm. 73% of RhB were decolored after 30 min of illumination.

The catalyst's lifetime is an important parameter of the photocatalytic process, so it is essential to evaluate the stability of photocatalyst for practical application. The recycling experiments on AS-50 sample were carried out under the same reaction conditions. After every 30 min of photodegradation, the separated photocatalysts were washed with deionized water and then dried. As Fig. 4a shows, the high photocatalytic performance of AgBr-$SmVO_4$ for RhB degradation was effectively maintained after 6 times cycle experiments, indicating that AgBr-$SmVO_4$ has high stability under visible-light irradiation. In addition to RhB, other dyes (MB, MO, and MG) and phenol were also degraded in the presence of AS-50 sample. The initial concentrations of all these dyes were 20 mmol/L. For phenol, much higher concentration (50 mmol/L) was adopted due to its weak signal in the UV–vis spectrum. The testing result is shown in Fig. 4b. AS-50 sample displays an adsorption capability with the sequence of MB > MG > RhB > MO for different dyes. After visible-light irradiation for 30 min, all concentrations of these dyes decreased to be lower than 7%, indicating that the AgBr-$SmVO_4$ composite had high photocatalytic efficiency for many dyes' degradation. Compared with the dyes, AS-50 sample exhibits lower photoactivity for phenol, which might be attributed to its bad adsorption for phenol and the high concentration of phenol. However, the great decrease in phenol content after 30 min of light irradiation can still convince us that the AgBr-$SmVO_4$ composite is an efficient photocatalyst. In addition, because phenol only responses to UV light (that's why P25 exhibits no photoactivity, See Fig. S5), the result proved that the donation of the dye photosensitization effect for the phoactivity of AgBr-$SmVO_4$ composite might be ignored.

In summary, the AgBr-$SmVO_4$ composite was an efficient photocatalyst for the degradation of RhB. $SmVO_4$ semiconductor exhibited great promotion effect. By controlling the influencing factors (AgBr-$SmVO_4$ amount and initial RhB concentration), the photocatalytic activity of the composite can be enhanced further.

Table 1
Specific surface area of AgBr-$SmVO_4$ composite catalysts.

Catalysts	AgBr	$SmVO_4$	AS-20	AS-40	AS-50	AS-60
$S/m^2/g$	0.2	73	26.9	8.6	3.8	2.2

In addition to the high photoactivity, the AgBr-$SmVO_4$ composite also presents the high stability, high complete oxidation ability, and the general applicability for dyes degradation.

3.2. Characterization of catalyst

The catalyst AgBr/$SmVO_4$ composite was characterized by BET surface area, XRD, XPS, SEM, TEM, DRS, and PT analysis. The BET surface areas of the AgBr-$SmVO_4$ composites are given in Table 1. The specific surface area of AgBr equals to 0.2 m^2/g which is dramatically lower than that of $SmVO_4$ (73 m^2/g). For AgBr-$SmVO_4$ composite, the BET value decreased from 26.9 to 2.2 m^2/g with the increase of AgBr content. AgBr-$SmVO_4$ composite have higher surface area than AgBr, which might be the reason of its stronger adsorption ability of RhB. However, the dye adsorption ability on catalyst is not always in agreement with its BET values. The adsorption of RhB on AgBr-$SmVO_4$ composite is stronger than $SmVO_4$, although $SmVO_4$ has the highest BET value in Table 1. Moreover, the photocatalytic activity is also inconsistent with the adsorption ability (See Fig. 1 and Fig. S1). The result indicated that the specific surface area or the dye adsorption ability was not a key factor affecting the photocatalytic activity of AgBr-$SmVO_4$ samples. The most important factor might be the catalyst composition.

Fig. 5 displays the XRD patterns of $SmVO_4$, AgBr, and AgBr-$SmVO_4$ composites. The patterns show that $SmVO_4$ crystal was in its tetragonal phase (PDF# 17-0876), while AgBr was of face-centered cubic structure (PDF# 06-0438). The AgBr/$SmVO_4$ composite consists of AgBr and $SmVO_4$. With the increase of AgBr content, the intensities of diffraction peaks of AgBr increased, whereas those of $SmVO_4$ decreased simultaneously. The XRD

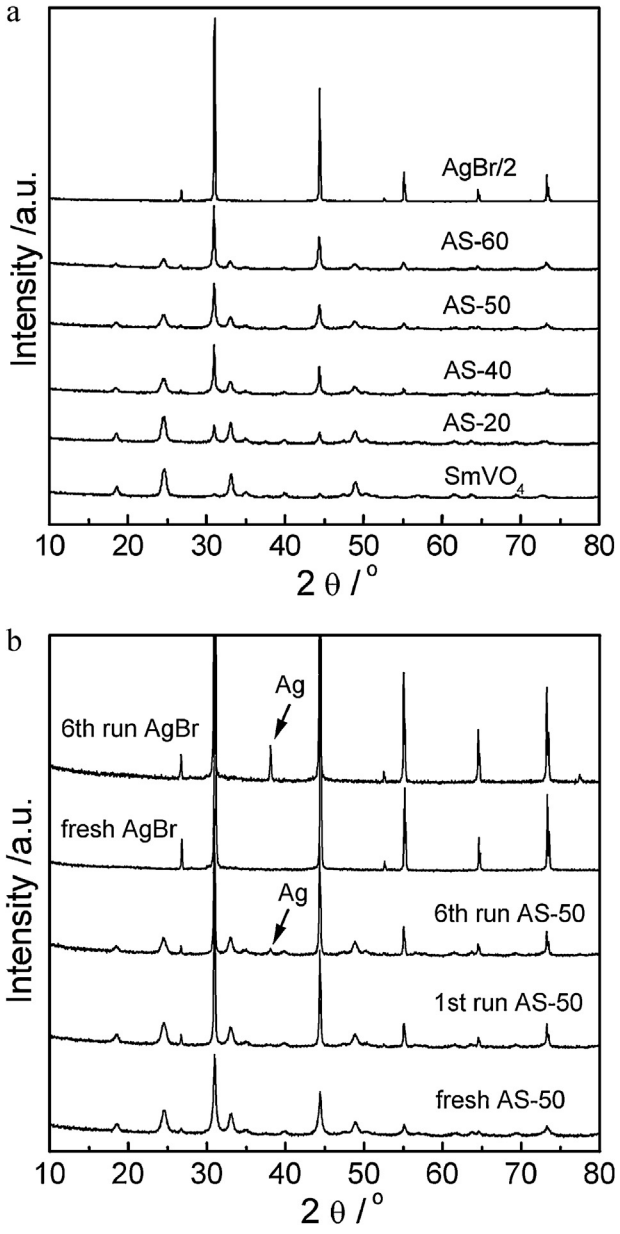

Fig. 5. XRD patterns of fresh AgBr, $SmVO_4$, Ag-AgBr-$SmVO_4$ photocatalysts (a) and the used AS-50 sample (b).

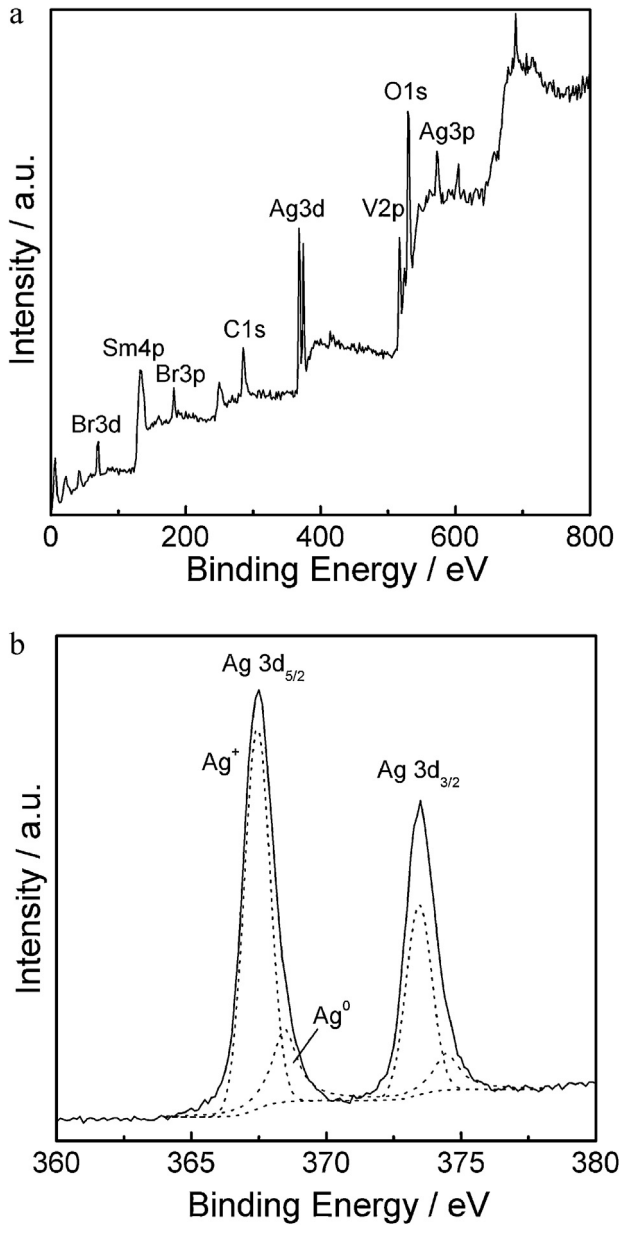

Fig. 6. XPS spectrum of used AS-50 sample (a) and the high-resolution XPS spectrum of Ag 3d (b).

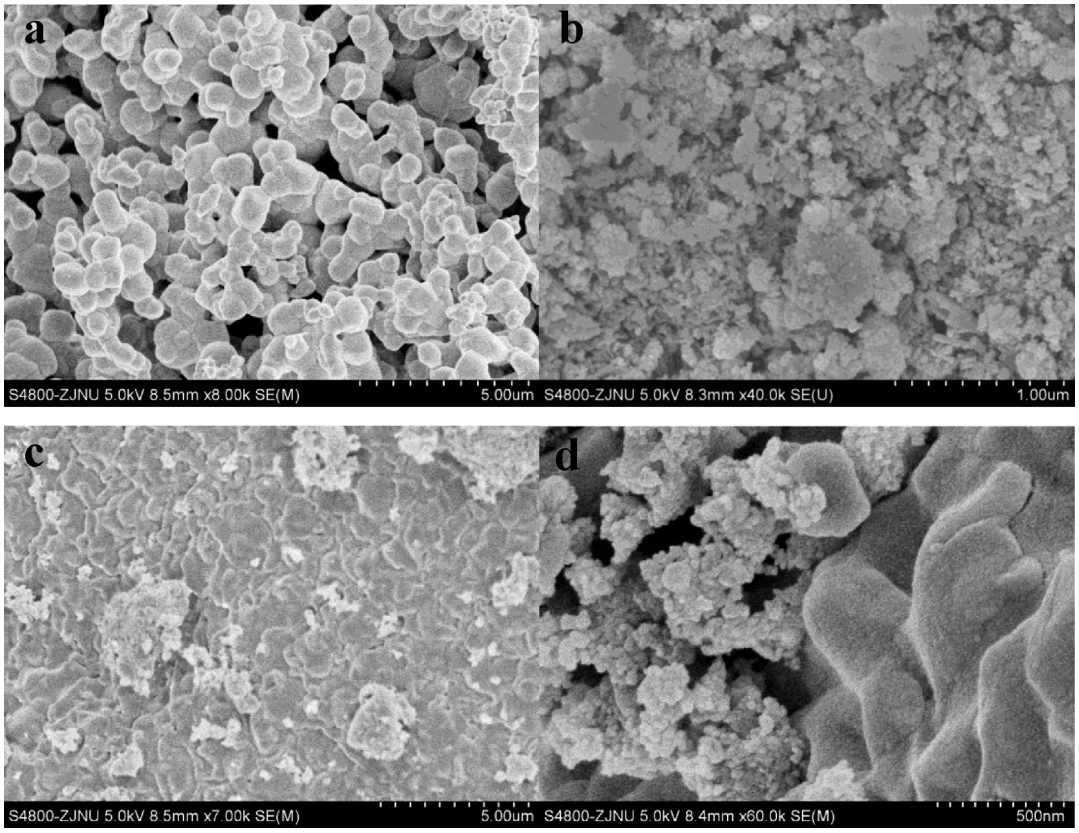

Fig. 7. SEM photograph of AgBr (a), $SmVO_4$ (b), and a representative catalyst AS-50 (c and d).

patterns of used AgBr and used AS-50 samples are shown in Fig. 5b. A small diffraction peak at 38.1° which could be assigned to the (1 1 1) face of metal Ag (PDF# 04-0783) was observed on the used AgBr sample. It indicated that AgBr was transformed to Ag/AgBr system during the photocatalytic reaction, which is consistent with the results observed in previous studies [15–20]. For AgBr/$SmVO_4$ composite, the metal Ag was also detected after the sample was used for six times. However, the characteristic peak of Ag is much lower than that of used AgBr, which might be attributed to that the coupled $SmVO_4$ suppressed the decomposition of AgBr.

The result in Fig. 5b shows that AS-50 sample used once displays the same XRD pattern with the fresh sample, which might be due to that the concentration of formed Ag is too low to be detected by XRD. The XPS technique is more sensitive than XRD. Therefore, it was used to verify the existence of metal Ag. Both signals of Sm, V, Ag, Br, O were detected in the XPS spectrum of used AS-50 sample (Fig. 6a). The binding energy of Sm $3d_{5/2}$, V$3d_{5/2}$, Br3d were determined to be 1083.6 eV, 517.1 eV, and 68.5 eV, respectively, indicating the existence of Sm^{3+}, V^{5+}, and Br^- (See Fig. S6) [19,30,31]. The high-resolution XPS spectrum of Ag 3d is shown in Fig. 6b. The binding energy of Ag $3d_{5/2}$ was observed at binding energies of 367.9 eV. It is reported that the Ag ($3d_{5/2}$) binding energies of Ag, Ag_2O and AgO were in the order: Ag (368.2 eV) >Ag_2O (367.8 eV) >AgO (367.4 eV) [32]. Therefore, trace metal Ag might exist in the used AgBr/$SmVO_4$ composite.

Fig. 7 shows the SEM images of AgBr, $SmVO_4$, and AS-50 composite samples. AgBr particles are much larger than $SmVO_4$. Due to the huge difference in particle size, the identification of AgBr or $SmVO_4$ from the SEM photograph of AgBr/$SmVO_4$ composite is easy. It can be seen that the small particles of $SmVO_4$ disperses in the AgBr. However, the dispersion is rather inhomogeneous. Many $SmVO_4$ nanoparticles are agglomerated, and so are the AgBr particles. Moreover, the melting of AgBr is observed due to the high calcination of 500 °C, which might be beneficial to form an AgBr–$SmVO_4$ heterojunction structure with efficient photoactivity. The TEM image of used AS-50 sample is shown in Fig. 8. The large particles with dark color can be assigned to AgBr, while the small particles can be ascribed to $SmVO_4$ based on the result of SEM experiment. This assignment is verified by the HR-TEM images shown in Fig. 8b. The big particle exhibits a lattice fringe with d = 0.284 nm, which matches the (2 0 0) crystallographic plane of AgBr. Another fringe with d = 0.364 nm belonged to the (2 0 0) crystallographic plane of tetragonal $SmVO_4$ can be observed in the jointed small particle. Moreover, the lattice fringe of metal Ag (d = 0.229 nm), which corresponds to the (1 1 1) crystallographic plane, is also observed. This result clearly shows the AgBr-$SmVO_4$ composite transformed to Ag-AgBr-$SmVO_4$ system, which is in good agreement with the XRD and XPS result. Besides, the three phases correlate well. This relationship would favor the formation of junctions, thereby improving the charge transfer between them.

The optical absorptions of the $SmVO_4$, AgBr and AgBr-$SmVO_4$ nanojunction system were measured using an UV–vis spectrometer, and the results are shown in Fig. 9. Both $SmVO_4$ and AgBr samples exhibit strong photoabsorption ability for visible light. The band gap of $SmVO_4$ and AgBr are determined to be 2.28 eV and 2.43 eV (see Fig. S7), respectively, which are consistent with the values previous reported [33,34]. The photoabsorption properties of AgBr-$SmVO_4$ composite is correlated with the AgBr content. With the increase of AgBr content, the light absorption ability is enhanced. AS-60 sample displays the highest photoabsorption performance. Fig. 9b shows the UV–vis spectra of used $SmVO_4$, AgBr, and AS-50 sample. No change is observed in the UV–vis spectrum of used $SmVO_4$. However, for the used AgBr and AS-50 samples, a strong absorption in the region of 450–800 nm is observed, which

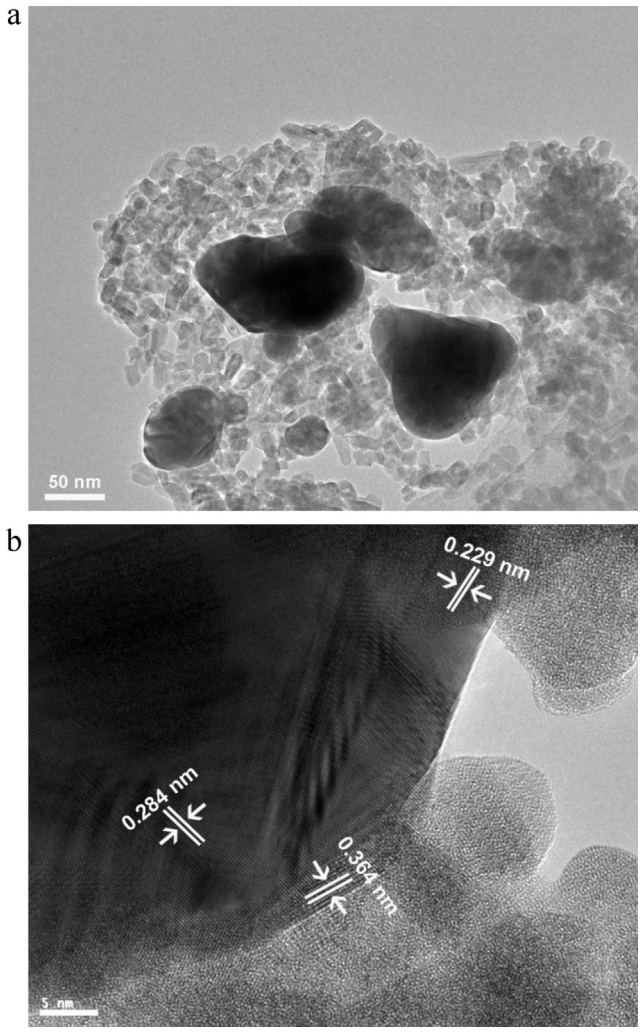

Fig. 8. TEM (a) and HR-TEM (b) images of used AS-50 photocatalyst.

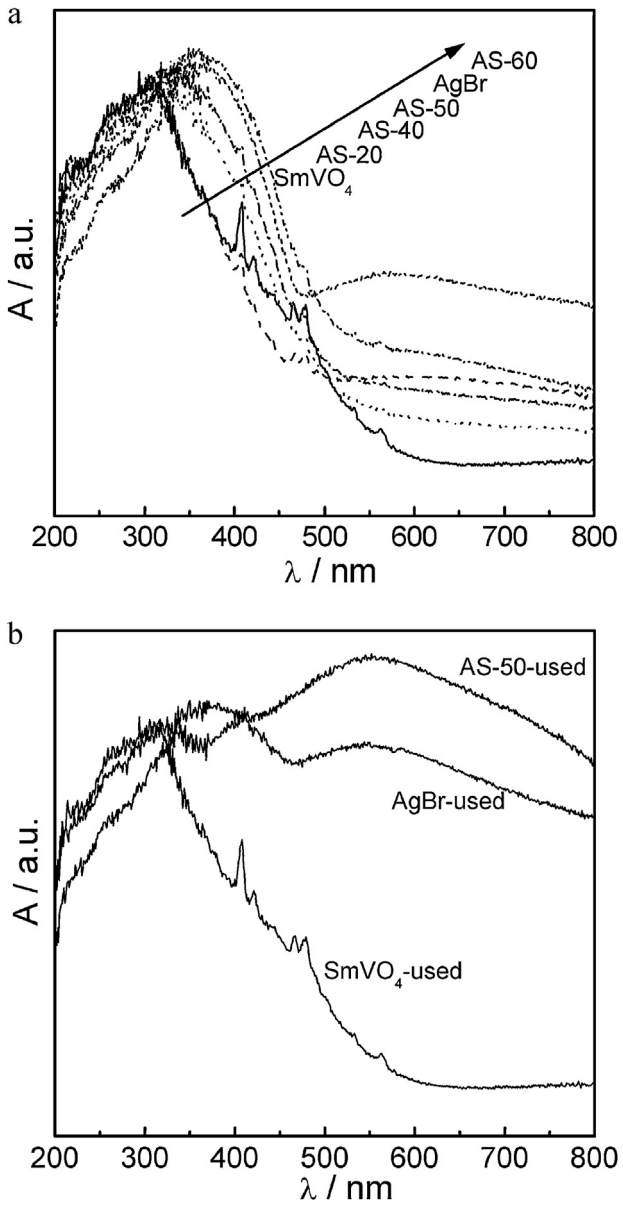

Fig. 9. UV–vis spectra of (a) fresh AgBr-$SmVO_4$ composites and (b) used photocatalys.

can be attributed to the surface plasmon absorption of Ag nanoparticles [6–8,11,12]. This result is in accordance with that of XRD, XPS, and TEM.

The above results shows that the AgBr-$SmVO_4$ composite is actual the Ag-AgBr-$SmVO_4$ nanojunction system during the photocatalytic reaction. Considering that the efficient separation of electron–hole pairs is widely accepted to be the key factor influencing the photocatalytic activity of composite catalyst, it can be deduced that the Ag-AgBr-$SmVO_4$ nanojunction system holds strong ability to restrain the recombination of electron–hole pairs, which results in its high photocatalytic activity. The electronic structures and energy band of visible-light-response component AgBr and $SmVO_4$ have been studied by some researchers [33,35]. AgBr presents the conduction band (CB) and valence band (VB) edge potential at −1.10 and 1.33 eV, respectively. For $SmVO_4$, the corresponding value is −0.29 and 1.99 eV, respectively, which is lower than that of AgBr. The suitably matching band indicates that the photoinduced electrons on the AgBr particle surface can easily transfer to $SmVO_4$ via the interfaces, while the holes on the $SmVO_4$ surface can migrate to AgBr in a similar manner. The charge transfer effectively suppresses the recombination of electron–hole pairs and, thereby improving the photo-oxidation efficiency. This mechanism can be verified by the photocurrent–time (PT) measurement which is generally regarded as the most efficient method to demonstrate the interfacial charge transfer dynamics in composite photocatalysts [36–38]. The high efficiency in the interfacial charge transfer would promote the e^-–h^+ separation efficiency, and thus result in the high photocurrent. Fig. 10 shows the photocurrent-time testing curves of AgBr and AS-50 composite. The AS-50 sample presents a much higher photocurrent than AgBr, indicating that the composite holds stronger ability in separation of electron–hole pairs. This is consistent with the analysis of the coupling effect of AgBr and $SmVO_4$, as discussed above.

Besides AgBr and $SmVO_4$, the Ag nanoparticles also play an important role in the photocatalytic reaction. This means that the high photocurrent of AS-50 sample in Fig. 10 contains the contribution of metal Ag. Several mechanisms have been proposed to explain the promotion effect of Ag nanoparticles in the Ag-AgX-semiconductors systems. Some researchers suggested that the Ag-AgBr-semiconductor system worked by the Z-scheme mechanism [13,34,39]. The metal Ag in the composite acts as a recombination centre for CB-electrons (coupled semiconductor) and VB-holes (AgBr), and contributes to enhancing interfacial charge transfer and realizing the complete separation of VB-holes (coupled semiconductor) and CB-electrons (AgBr). In addition,

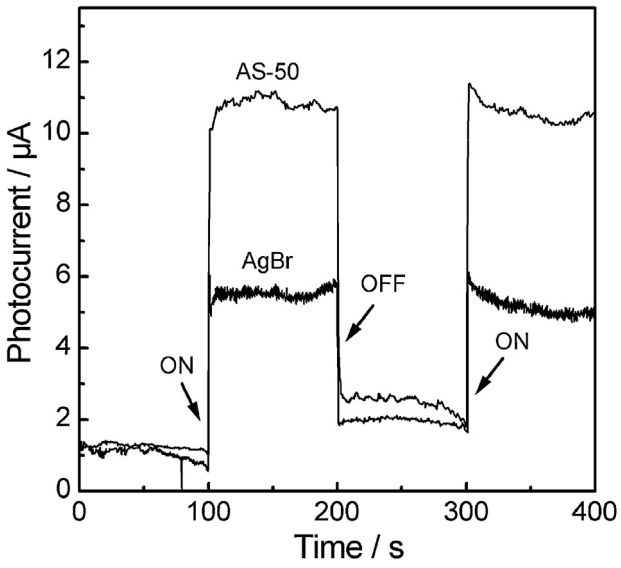

Fig. 10. Transient photocurrent response for AgBr, and AS-50 photocatalyst.

some other researchers suggested that Ag nanoparticles could absorb visible light and generate electron and holes due to the surface plasmon effect. These plasmon-induced charges could contribute the photocatalytic degradation of dyes [5–7,40]. With the exception of the above two proposed mechanisms, it is widely accepted that Ag nanoparticles can enhance charge separation through acting as "electron sinks" [41,42]. The photoinducted electron generated in AgX or another semiconductor can migrate to Ag nanoparticle, and thereby promote the photocatalytic efficiency. In the current case of Ag-AgBr-$SmVO_4$ system, it is believed that the metal Ag might work through the last two mechanisms. The catalytic testing results showed that Ag-AgBr-$SmVO_4$ system displayed the photoactivity under light with $\lambda > 565$ nm. The cut-off wavelength was higher than the band gap edge of AgBr or $SmVO_4$, suggesting that the high photoactivity originated from the plasmon-induced electrons and holes of Ag nanoparticles. It is clear that Ag is not the recombination centre of charges and the Ag-AgBr-$SmVO_4$ system does not follow the Z-scheme mechanism. The proposed photocatalytic process of Ag-AgBr-$SmVO_4$ nanojunction system is shown in Fig. 11.

Therefore, it can be concluded that the Ag-AgBr-$SmVO_4$ nanojunction system can separate the photoexcited electron and holes efficiently by the charge transfer at the interface of the three phases. The AS-50 sample might contain a suitable concentration of Ag, AgBr, and $SmVO_4$. It caused the well dispersion of the consisted phases in composite and generated the highest amounts of interface, which favored the transfer and separation of the charge carriers and consequently resulted in the highest photocatalytic activity. Under the synergetic actions of Ag, AgBr, and $SmVO_4$, the electrons are accumulated on Ag nanoparticles, while the holes are mainly on the valence band of $SmVO_4$. These electrons and holes have strong reducibility and oxidation ability. However, they usually did not react with the organic dyes directly. Instead, some active species (such as •OH and $•O_2^-$) were first formed through the reaction of charges and adsorbed H_2O or O_2. For various photocatalyst, the main active species is usually varied due to the difference in their band structure or phase composition. Therefore, different scavenges used as probes were introduced into the photocatalytic degradation of RhB in order to determine the reactive species. As shown in Fig. 12, isopropanol (IPA, a quencher of •OH) [26,27] has no effect on the degradation of RhB, indicating the •OH is not the reactive species. This result is also verified by the TA-PL probing measurement (See Fig. 13). No PL signal at approximately 425 nm is

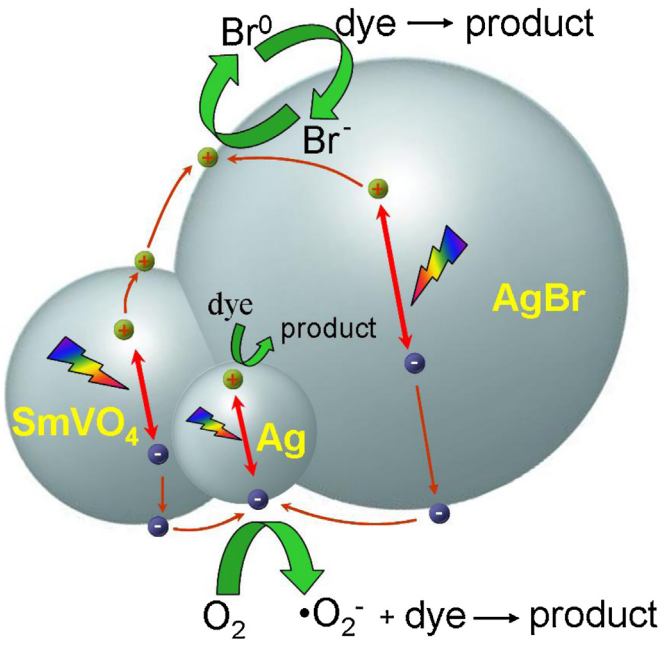

Fig. 11. Scheme for electron–hole separation and transport at the interface of Ag-AgBr-$SmVO_4$ composite photocatalyst.

observed with the increase of irradiation time, which demonstrates that no •OH radicals were formed during the photocatalytic oxidation process. Different from IPA, the addition of benzoquinone (BQ, $•O_2^-$ scavenger) and (AO, h^+ scavenger) decreases the photocatalytic activity [26,27]. In general, the more reduced photoactivity the more important the role the reactive species in the reaction. The result in Fig. 12 suggests that $•O_2^-$ was the main reactive species for the degradation of RhB. However, it should be noted that the suppression of BQ in photoactivity is not so great, which indicates there might exist another important reactive species. Considering that the holes accumulated on the VB of AgBr can oxidize Br^- ions to Br^0 atoms, it can be deduced that Br^0 atoms are the reactive radical species and degrade RhB [7,8,17]. This inference also explained why the holes show a minor effect on the degradation of RhB.

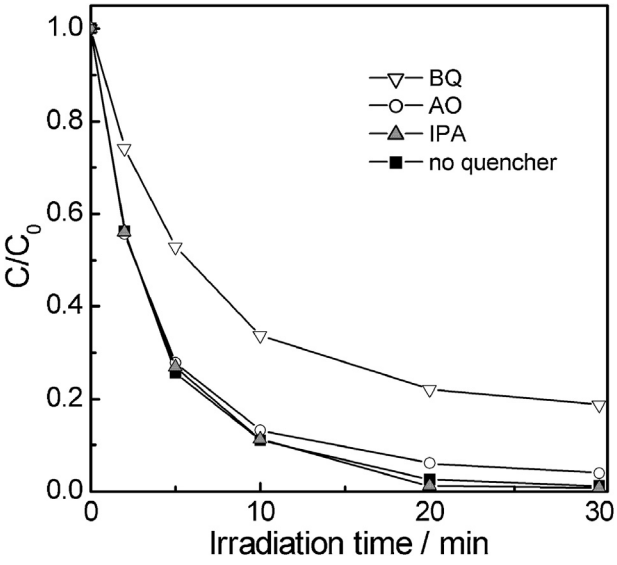

Fig. 12. Photocatalytic activity of AgBr-$SmVO_4$ photocatlalysts with different quenchers.

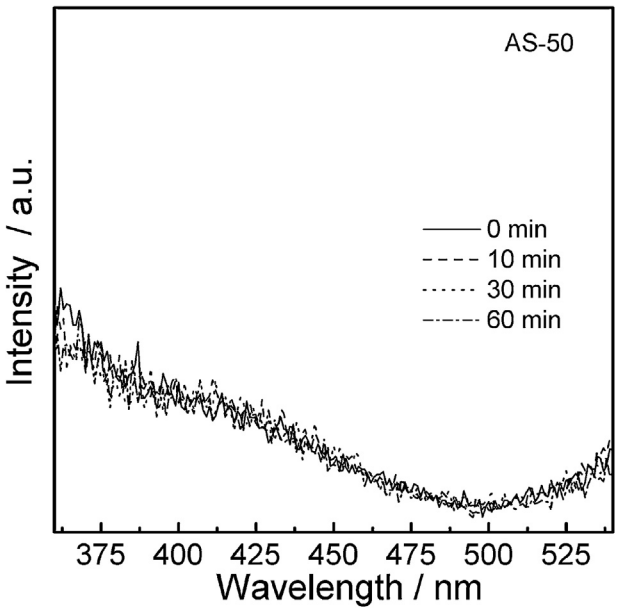

Fig. 13. •OH-trapping photoluminescence spectra of AS-50 sample under visible light irradiation in a solution of terephthalic acid at room temperature.

4. Conclusions

In summary, AgBr/$SmVO_4$ composite was prepared using a facile deposition method. The as-prepared powders exhibited excellent performance on the degradation of RhB, and displayed much higher photocatalytic activity than single AgBr or $SmVO_4$ under visible-light irradiation (>420 nm). Besides, the AgBr-$SmVO_4$ composite showed high stability. After 6 cycles of repetition tests, the degradation efficiency of RhB still remained 99.0%. Structural characterization suggested that the AgBr-$SmVO_4$ composite transformed to the Ag-AgBr-$SmVO_4$ system during the photocatalytic reaction. The synergy effect of the Ag, AgBr, and $SmVO_4$ was considered as the origin of the high activity of AgBr-$SmVO_4$ composite. This study demonstrated that the synthesized AgBr-$SmVO_4$ photocatalyst might be a promising efficient composite photocatalyst for environmental purification due to its high activity, stability, complete oxidation ability, and the general applicability for dyes degradation. Of course, the high content of AgBr would greatly increase the catalyst cost. Further efforts should be done before the AgBr-$SmVO_4$ catalyst could be applied in practice.

Acknowledgements

This work was financially supported by the National Natural Science Foundation of China (21003109, 51108424), the program for Changjiang Scholars and Innovative Research Team in Chinese Universities (IRT0980), the program for Zhejiang Leading Team of Science and Technology Innovation (2009R50020), the Opening-foundation of State Key Laboratory Physical Chemistry and Solid Surfaces, Xiamen University, China (201311), and the Science Foundation of Zhejiang Normal University (KJ20120028).

Appendix A. Supplementary data

Supplementary data associated with this article can be found, in the online version, at http://dx.doi.org/10.1016/j.apcatb.2013.02.024.

References

[1] B. Ohtani, Journal of Photochemistry and Photobiology C: Photochemistry Reviews 11 (2010) 157–178.
[2] S. Malato, J. Blanco, A. Vidal, C. Richter, Applied Catalysis B: Environmental 37 (2002) 1–15.
[3] A. Fujishima, T.N. Rao, D.A. Tryk, Journal of Photochemistry and Photobiology C: Photochemistry Reviews 1 (2000) 1–21.
[4] K. Nakata, A. Fujishima, Journal of Photochemistry and Photobiology C: Photochemistry Reviews 13 (2000) 169–189.
[5] P. Wang, B.B. Huang, X.Y. Qin, X.Y. Zhang, Y. Dai, J.Y. Wei, M.H. Whangbo, Angewandte Chemie-International Edition 47 (2008) 7931–7933.
[6] P. Wang, B.B. Huang, Z.Z. Lou, X.Y. Zhang, X.Y. Qin, Y. Dai, Z.K. Zheng, Z.Y. Wang, X.N. Wang, Chemistry-A European Journal 16 (2010) 538–544.
[7] P. Wang, B.B. Huang, X.Y. Zhang, X.Y. Qin, H. Jin, Y. Dai, Z.Y. Wang, J.Y. Wei, J. Zhan, S.Y. Wang, J.P. Wang, M.H. Whangbo, Chemistry-A European Journal 15 (2009) 1821–1824.
[8] J. Jiang, H. Li, L.Z. Zhang, Chemistry-A European Journal 18 (2012) 6360–6369.
[9] S. Ghosh, A. Saraswathi, S.S. Indi, S.L. Hoti, H.N. Vasan, Langmuir 28 (2012) 8550–8561.
[10] N. Kakuta, N. Goto, H. Ohkita, T. Mizushima, The Journal of Physical Chemistry B 103 (1999) 5917–5919.
[11] M.J. Kerker, Journal of Colloid and Interface Science 105 (1985) 297–314.
[12] S.M. Sun, W.Z. Wang, L. Zhang, M. Shang, L. Wang, Catalysis Communications 11 (2009) 290–293.
[13] X.F. Wang, S.F. Li, Y.Q. Ma, H.G. Yu, J.G. Yu, The Journal of Physical Chemistry C 115 (2011) 14648–14655.
[14] M.A. Asi, C. He, M.S. Su, D.H. Xia, L. Lin, H.Q. Deng, Y. Xiong, R.L. Qiu, X.Z. Li, Catalysis Today 175 (2011) 256–263.
[15] J. Cao, B.D. Luo, H.L. Lin, S.F. Chen, Journal of Hazardous Materials 190 (2011) 700–706.
[16] B. Ma, J.F. Guo, W.L. Dai, K.N. Fan, Applied Catalysis B: Environmental 123–124 (2012) 193–199.
[17] Z.J. Zhou, M.C. Long, W.M. Cai, J. Cai, Journal of Molecular Catalysis A: Chemical 353–354 (2012) 22–28.
[18] S.B. Sun, X.T. Chang, L.H. Dong, Y.D. Zhang, Z.J. Li, Y.Y. Qiu, Journal Solid State Chemistry 184 (2011) 2190–2195.
[19] H. Xu, J. Yan, Y.G. Xu, Y.H. Song, H.M. Li, J.X. Xia, C.J. Huang, H.L. Wan, Applied Catalysis B: Environmental 129 (2013) 182–193.
[20] W. Xiong, Q.D. Zhao, X.Y. Li, D.K. Zhang, Catalysis Communications 16 (2011) 229–233.
[21] K. Vignesh, A. Suganthi, M. Rajarajan, S.A. Sara, Powder Technology 224 (2012) 331–337.
[22] H. Zhang, X.F. Fan, X. Quan, S. Chen, H.T. Yu, Environmental Science and Technology 45 (2011) 5731–5736.
[23] Y.M. He, T.L. Sheng, J.S. Chen, R.B. Fu, S.M. Hu, X.T. Wu, Catalysis Communications 10 (2009) 1354–1357.
[24] Y.J. Wang, Y.M. He, T.T. Li, J. Cai, M.F. Luo, L.H. Zhao, Chemical Engineering Journal 189–190 (2012) 473–481.
[25] M.C. Long, W.M. Cai, H. Kisch, The Journal of Physical Chemistry C 112 (2008) 548–554.
[26] G.T. Li, K.H. Wong, X.W. Zhang, C. Hu, J.C. Yu, R.C.Y. Chan, P.K. Wong, Chemosphere 76 (2009) 1185–1191.
[27] J. Cao, B.Y. Xu, B.D. Luo, H.L. Lin, S.F. Chen, Applied Surface Science 257 (2011) 7083–7089.
[28] D.Z. Li, Z.X. Chen, Y.L. Chen, W.J. Li, H.J. Huang, Y.H. He, X.Z. Fu, Environmental Science and Technology 42 (2008) 2130–2135.
[29] R. Jiang, H.Y. Zhu, X.D. Li, L. Xiao, Chemical Engineering Journal 152 (2009) 537–542.
[30] B.V. Kumara, R. Velchuria, G. Prasadb, B. Sreedharc, K. Ravikumard, M. Vithala, Ceramics International 36 (2010) 1347–1355.
[31] S. Beke, L. Kőrösi, S. Papp, A. Oszkó, L. Nánai, Applied Surface Science 255 (2009) 9779–9782.
[32] X.F. Zhang, Y.B. Zhang, X. Quan, S. Chen, Journal of Hazardous Materials 167 (2009) 911–914.
[33] T.T. Li, Y.M. He, L.H. Zhao, J. Cai, M.F. Luo, J.J. Lin, Applied Catalysis B: Environmental 129 (2013) 255–263.
[34] H.L. Lin, J. Cao, B.D. Luo, B.Y. Xu, S.F. Chen, Catalysis Communications 21 (2012) 91–95.
[35] L.S. Zhang, K.H. Wong, Z.G. Chen, J.C. Yu, J.C. Zhao, C. Hu, C.Y. Chan, P.K. Won, Applied Catalysis A: General l 363 (2009) 221–229.
[36] M. Kong, Y.Z. Li, X. Chen, T.T. Tian, P.F. Fang, F. Zheng, X.J. Zhao, Journal of The American Chemical Society 133 (2011) 16414–16417.
[37] Q.J. Xiang, J.G. Yu, M. Jaroniec, The Journal of Physical Chemistry C 115 (2011) 7355–7363.
[38] Z.Y. Li, B. Gao, G.Z. Chen, R. Mokaya, S. Sotiropoulos, G.L. Puma, Applied Catalysis B: Environmental 110 (2011) 50–57.
[39] K.P. Xie, Q. Wu, Y.Y. Wang, W.N. Guo, M.Y. Wang, L. Sun, C.J. Lin, Electrochemistry Communications 13 (2011) 1469–1472.
[40] K. Awazu, M. Fujimaki, C. Rockstuhl, J. Tominaga, H. Murakami, Y. Ohki, N. Yoshida, T. Watanabe, Journal of The American Chemical Society 130 (2008) 1676–1680.
[41] S. Krejčíková, L. Matějová, K. Kočí, L. Obalová, Z. Matěj, L. Čapek, O. Šolcová, Applied Catalysis B: Environmental 111–112 (2012) 119–125.
[42] Y.C. Lin, H.S. Lee, Journal of Hazardous Materials 179 (2010) 462–470.